Bioprocess and Biosystems Engineering (2024) 47:1515–1531
https://doi.org/10.1007/s00449-024-03046-9

RESEARCH PAPER

Green NiO nanoparticle-integrated PVA–alginate hydrogel: potent nanocatalyst for efficient reduction of anthropogenic water pollutants

Ganeswar Dalei[1] · Monalisa Jena[1] · Debasis Jena[2] · Navneel Kaur[1] · M. Swadhin Shakti Prasad[1] · Ayushman Sahu[1] · Bijnyan Ranjan Das[1] · Subhraseema Das[1,2]

Received: 2 April 2024 / Accepted: 11 June 2024 / Published online: 21 June 2024

Abstract

Hydrogel nanocatalyst composed of nickel oxide (NiO) nanoparticles embedded in PVA–alginate hydrogels were potentially explored toward the reduction of anthropogenic water pollutants. The NiO nanoparticles was accomplished via green method using waste pineapple peel extract. The formation of the nanoparticles was affirmed from different analytical techniques such as UV–Vis, FTIR, XRD, TGA, FESEM, and EDS. Spherical NiO nanoparticles were obtained having an average size of 11.5 nm. The nano NiO were then integrated into PVA–alginate hydrogel matrix forming a nanocomposite hydrogel (PVALg@ NiO). The integration of nano NiO rendered an improved thermal stability to the parent hydrogel. The PVALg@ NiO hydrogel was utilized as a catalyst in the reduction of 4-nitrophenol (4-NP), potassium hexacyanoferrate (III), rhodamine B (RhB), methyl orange (MO), and malachite green (MG) in the presence of a reducing agent, i.e., $NaBH_4$. Under optimized conditions, the reduction reactions were completed by 4.0 min and 3.0 min for 4-NP and potassium hexacyanoferrate (III), respectively, and the rate constant was estimated to be 1.14 min^{-1} and 2.15 min^{-1}. The rate of reduction was found to be faster for the dyes and the respective rate constants were be 0.17 s^{-1} for RhB, MG and 0.05 s^{-1} for MO. The PVALg@ NiO hydrogel nanocatalyst demonstrated a recyclability of four runs without any perceptible diminution in its catalytic mettle. The efficacy of the PVALg@ NiO hydrogel nanocatalyst was further examined for the reduction of dyes in real water samples collected from different sources and the results affirm its high catalytic potential. Thus, this study paves the path for the development of a sustainable hydrogel nanocatalyst for reduction of hazardous pollutants in wastewater treatment.

Graphical Abstract

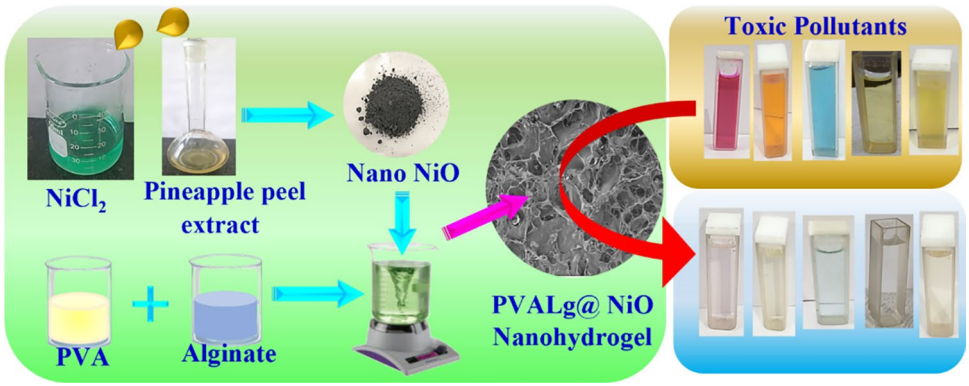

Keywords Green NiO nanoparticles · PVA– alginate hydrogel · Nanocatalyst · Catalytic reduction · Water pollutants

Extended author information available on the last page of the article

Introduction

Environmental pollution due to unregulated release of chemicals/effluents in urban wastewater has catapulted into a major threat to aquatic ecosystems across the globe. Among the diverse category of pollutants, nitro compounds and particularly 4-nitrophenol (4-NP) pose a severe threat to environment owing to its and toxicity and resilience to degradation [1]. Dyes are specifically another class of pollutants that impact the environment harshly. They are toxic and, in most cases carcinogenic, contribute largely to environmental deterioration. As the aforementioned pollutants are persistent in the environment both chemically and physiologically, their degradation becomes an uphill task. The conventional processes of elimination of these pollutants involve adsorption [2, 3], reverse osmosis [4], chemical coagulation [5] and photodegradation [6–10]. However, these methods proceed slow, generate secondary pollutant, have poor removal efficacy, and uneconomical in nature [11]. Thus, current times call in for simple yet proficient method for mitigation of such pollutants.

Of late, catalytic reduction of pollutants has blossomed into an enticing approach. Catalytic reduction has surged owing to its simplistic, fast, and cost-effective attributes [12]. A recyclable and stable catalyst is the need of the hour owing to sustainable and green chemistry. In this context, metal and/or metal oxide nanoparticles have blossomed as novel nanocatalysts for the reduction of diverse pollutants including nitro aromatic compounds, dyes, and heavy metals [13–15]. Even metallic nanoparticles have demonstrated overwhelming potential in electrocatalytic reduction of halogenated organic compounds in wastewater treatment [16]. Nonetheless, despite huge potency, pristine nanoparticles mostly occur in powder form and there arises certain inherent shortcomings while working with a powder catalyst; (a) difficulties in collection and separation of the catalyst post-reaction completion, (b) post-reaction recycling, and (c) difficulties in regulating the leaching of catalyst [17]. Therefore, anchoring nanoparticles onto a support system is usually warranted to accomplish their full catalytic potential. Concerning this, hydrogel-based nanocatalysts have witnessed a tremendous upthrust recently toward the catalytic reduction of pollutants.

Hydrogels are three-dimensional crosslinked polymeric networks comprising a water-insoluble matrix. Hydrogels designed from natural polymers have gained momentum as they are biocompatible and biodegradable in nature. Sodium alginate, a biopolymer mainly extracted from brown algae, has been greatly utilized in hydrogel synthesis. Alginate-based hydrogels have profound biomedical [18] and environmental [19] applications. Yet, at most times, pristine alginate films are fragile and lose their initial mechanical strength over time [20, 21]. Thus, alginate has been formulated into composite with other polymers to form an interpenetrating network. Polyvinyl alcohol (PVA) is a widely recognized polymer of eminence in health [22] and adsorbent for environmental mitigation [23]. Thus, integration of alginate and PVA has invariably led to composite systems endowed with improved physicochemical features apt for drug delivery [21], wound healing [24], 3D bioprinting [25], anticancer therapy [26], and adsorbent for removal of aromatic compounds [27] and heavy metals like Cu (II) and U (VI) [28]. Despite vast literature on PVA–alginate hydrogels, there has been no report on nanocomposite hydrogels of PVA–alginate as a catalyst toward the reduction of pollutants in wastewater treatment. Thus, the scarcity of reports in this direction has motivated us to explore the efficacy of PVA–alginate hydrogel nanocatalyst for reduction of pollutants.

In the current research contribution, nanocomposite hydrogels of nickel oxide nanoparticles (NiO NPs) integrated in PVA–alginate hydrogels were investigated for reduction of hazardous water pollutants (Scheme 1). To begin with, biogenic synthesis of NiO NPs was accomplished from waste pineapple peel extract via the environmentally benign microwave method. The NiO NPs were then incorporated onto PVA–alginate hydrogels and their thermal properties were examined. The designed nanocomposite hydrogel was utilized as a catalyst toward the reduction of pollutants like 4-nitrophenol (4-NP), potassium hexacyanoferrate (III) and organic dyes. Moreover, the re-usability and stability of our fabricated hydrogel nanocatalyst were also assessed. The efficacy of dye removal was further examined in real water samples to validate the practical applicability of our designed nanocatalyst hydrogel.

Materials and methods

Material procurement

Fresh pineapples were bought from local markets in Bhubaneswar. PVA (M_w = 89,000–98,000; 99.0% hydrolyzed), sodium alginate (viscosity 15–25 cp), 4-NP, $K_3[Fe(CN)_6]$ and the dyes were procured from Sigma-Aldrich, India and used as received. Sodium borohydride and nickel chloride were obtained from Merck, India and used as such.

Biogenic synthesis of NiO NPs from pineapple peel extract

The pineapples peels were cleaned, chopped into small pieces, and pulverized to obtain a powder. An hydroethanolic

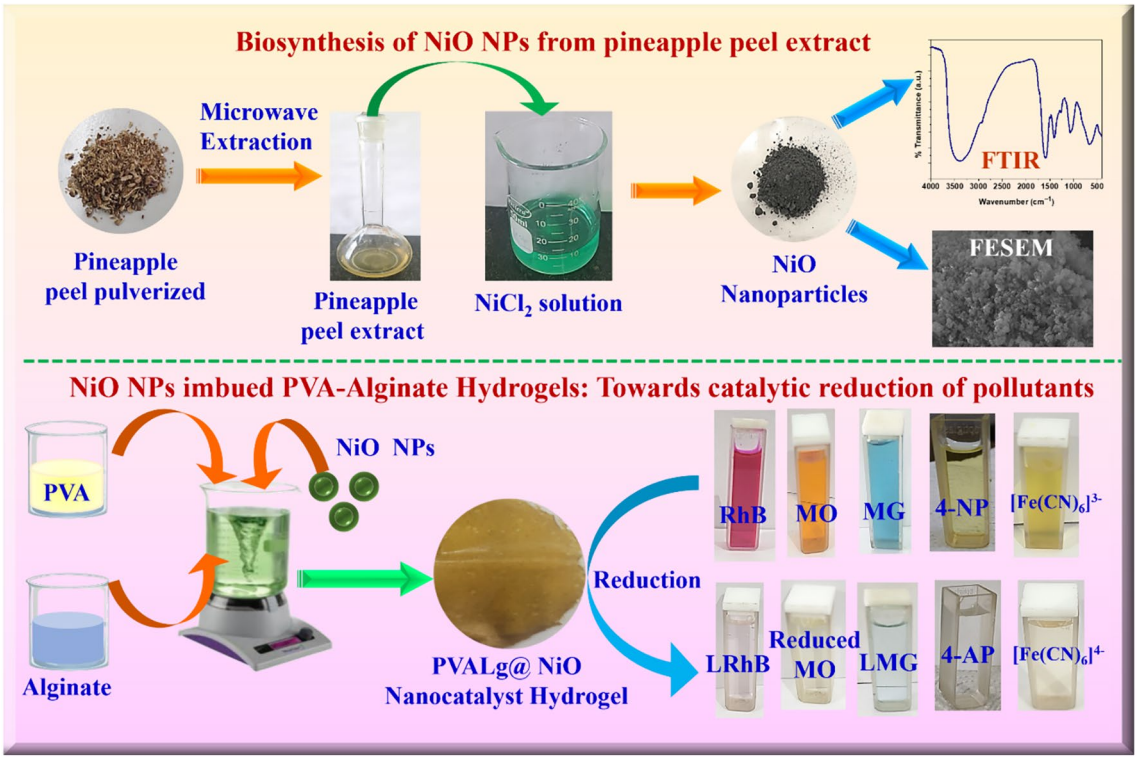

Scheme 1 Schematic depiction of biosynthesis of NiO nanoparticles from pineapple peel extract. The nano NiO was integrated into PVA–alginate hydrogels to form nanocomposite hydrogel (PVALg@ NiO). The potential of the PVALg@ NiO hydrogel nanocatalyst toward reduction of 4-NP, $K_3[Fe(CN)_6]$, rhodamine B (RhB), methyl orange (MO), and malachite green (MG) was assessed

solution (80% v/v) of the peel powder (1 g/50 mL) was subjected to microwave irradiation (Sineo UWave-1000 Microwave; 300 W; 10 min). The solution was filtered and the fresh extract was used for the biosynthesis of NiO NPs.

The biogenic synthesis of NiO NPs was performed as per reported procedure with slight modifications [29]. Briefly, 50 mL (5 mM) of aqueous nickel chloride solution was added to 20 mL of extract and mechanically agitated for few hours at 100 °C. Then the obtained precipitate was centrifuged for 20 min and washed thrice with distilled water. The collected NiO NPs was dried, ground and stored for further uses.

Synthesis of PVALg@ NiO nanocomposite hydrogel

PVA (10 wt%) and alginate (10 wt%) were dissolved separately in distilled water. They were then mixed together and agitated for a brief period to obtain a homogeneous solution. To this solution, NiO NPs (0.5 wt%) dispersed in water separately was added and further mechanically agitated (350 rpm) for 3 h. The gel solution was then casted to obtain the PVALg@ NiO nanocomposite hydrogel. Blank hydrogel (PVALg), devoid of NiO NPs, was also obtained in a similar manner.

Instrumentation and characterization

The FTIR spectra of the hydrogels were recorded in the range of 4000–400 cm^{-1} in a Thermo Nicolet iS5 FTIR spectrophotometer. The XRD profiles were collected on a RIGAKU ULTIMA–IV X-Ray diffractometer using Ni-filtered Cu Kα radiation (1.54 Å) and scanned from 5° to 85° at a rate of 3°/min. The thermogravimetric analysis (TGA) of samples was measured in a Perkin Elmer Simultaneous Thermal Analyzer system (STA 6000) under N_2 atmosphere (10 mL/min). The samples were heated from ambient temperature to 900 °C at a rate of 10 °C/min. The morphology of the samples was visualized on a Carl Zeiss-Gemini FESEM 300. The UV–Vis measurements were recorded in a Cary 100 UV–Vis spectrophotometer, Agilent Technologies.

Catalytic reduction

The catalytic reduction of 4-nitrophenol (4-NP), potassium hexacyanoferrate (III), and three organic dyes, namely rhodamine B (RhB), malachite green (MG), and methyl orange (MO) was investigated. The standard solutions of the aforesaid pollutants were prepared and the test was performed using $NaBH_4$ as a reducing agent. Briefly, 2 mL of each pollutant was taken in a cuvette and 1 mL of $NaBH_4$ was added

to it. To this, the hydrogel nanocatalyst was added and the reaction was observed spectrophotometrically. The percent reduction was calculated from initial and final concentrations of pollutants.

For reusability studies, the hydrogels were collected after each experiment, washed with distilled water and then reused for next experimental batch.

Kinetics

The pseudo-first-order formula equation was used to measure the reduction rate kinetics which is given by Eq. (1):

$$r = \ln\frac{c_t}{c_0} = \ln\frac{A_t}{A_0} = -k_{app}t, \quad (1)$$

where r is the rate of reduction, t is the reaction time, C_t represents the concentration of pollutant which corresponds to absorbance at any time t and the initial concentration is represented as C_0 which refers to absorbance at time 0. The linear relationships of reaction time (t) *vs.* ln (C_t/C_0) were plotted for reduction reactions by PVALg@ NiO hydrogel nanocatalyst and the slopes of the plots provided the respective the apparent rate constants (k_{app}).

Results and discussion

Biosynthesis of NiO NPs from pineapple peel extract

Biosynthesis of NiO NPs from pineapple peel extract is a simplistic, economic, and ecofriendly method and avoids the use of noxious chemicals. In this study, NiO NPs were synthesized from waste pineapple peel extract. A color change was detected when nickel chloride solution was added to the extract from aqua green to brownish black. Since the extract is endowed with diverse phytocompounds comprising flavonoids, alkaloids, phenols, terpenoids, essential oils, etc. that behave as reducing, capping, and stabilizing agents; the reduction of nickel chloride to nano NiO is accomplished [30]. The formation of NiO NPs was ascertained from UV–Vis, FTIR, XRD, TGA, SEM, and EDS analyses, described below.

UV–Vis analysis

The UV–Vis spectroscopy was performed to confirm the formation of NiO NPs by the green method. The UV–Vis spectrum of the synthesized nano NiO is depicted in Fig. 1A. The strong absorption band at 300 nm affirmed the formation of NiO NPs. This result corroborates with other reported data [29, 31].

FTIR analysis

FTIR spectroscopy depicts to find out the possible active biomolecules in the plant extract and identify the functional groups present in the green-synthesized NiO NPs. From Fig. 1B, the band observed at 3394 cm^{-1} was accredited to the O–H_{str} of phenols/alcohol. The band at 1603 cm^{-1} was assigned to H–O–H bending vibrations [29]. These bands indicate the presence of moisture. The key absorption peak of the NiO NPs bond was witnessed at 660 cm^{-1} which is in accordance with earlier reports [29, 32].

XRD analysis

The X-Ray diffraction patterns of the synthesized NiO NPs has been projected in Fig. 1C. The peak positions corresponding to $2\theta = 37.4°$, 43.4°, 63.0°, 75.5°, and 79.8° could be indexed as (111), (200), (220), (311), and (222) crystal planes of the bulk NiO, respectively, which agrees well with the standard data (JCPDS card no. 47-1049) [33, 34]. The presence of sharp peaks put forth the highly crystalline nature of our prepared nano NiO sample. The crystallite size of the NiO NPs calculated from Scherrer formula was estimated to be 11.5 nm.

Thermogravimetric analysis

To infer the changes occurring during thermal treatment of the $NiCl_2$ precursor, thermogravimetric analysis (TGA) was studied from ambient temperature to 900 °C in nitrogen environment. Figure 1D depicts the TG thermogram of the biosynthesized NiO NPs. It was clearly noted that the weight loss was inclusive of three steps. The region of first weight loss was detected in the range of 25–220 °C that could be attributed to the vaporization of water molecules associated with the precursor sample. The second region of weight loss was marked in the range of 220–420 °C that could be linked with the thermal decomposition of $NiCl_2$ to NiO nanoparticles. Beyond this temperature, a near negligible increase in weight loss was witnessed indicating the completion of the formation of NiO NPs [34–36].

Analyses of morphology and elemental compositions

The morphology of our prepared NiO NPs was envisaged by FESEM and the elemental composition was observed by EDS. From Fig. 2A, it was witnessed that the NiO NPs have spherical shape. Furthermore, the elemental analysis in Fig. 2B revealed the composition of Ni and O in NiO NPs to be 43.3% and 56.7% by mass, respectively.

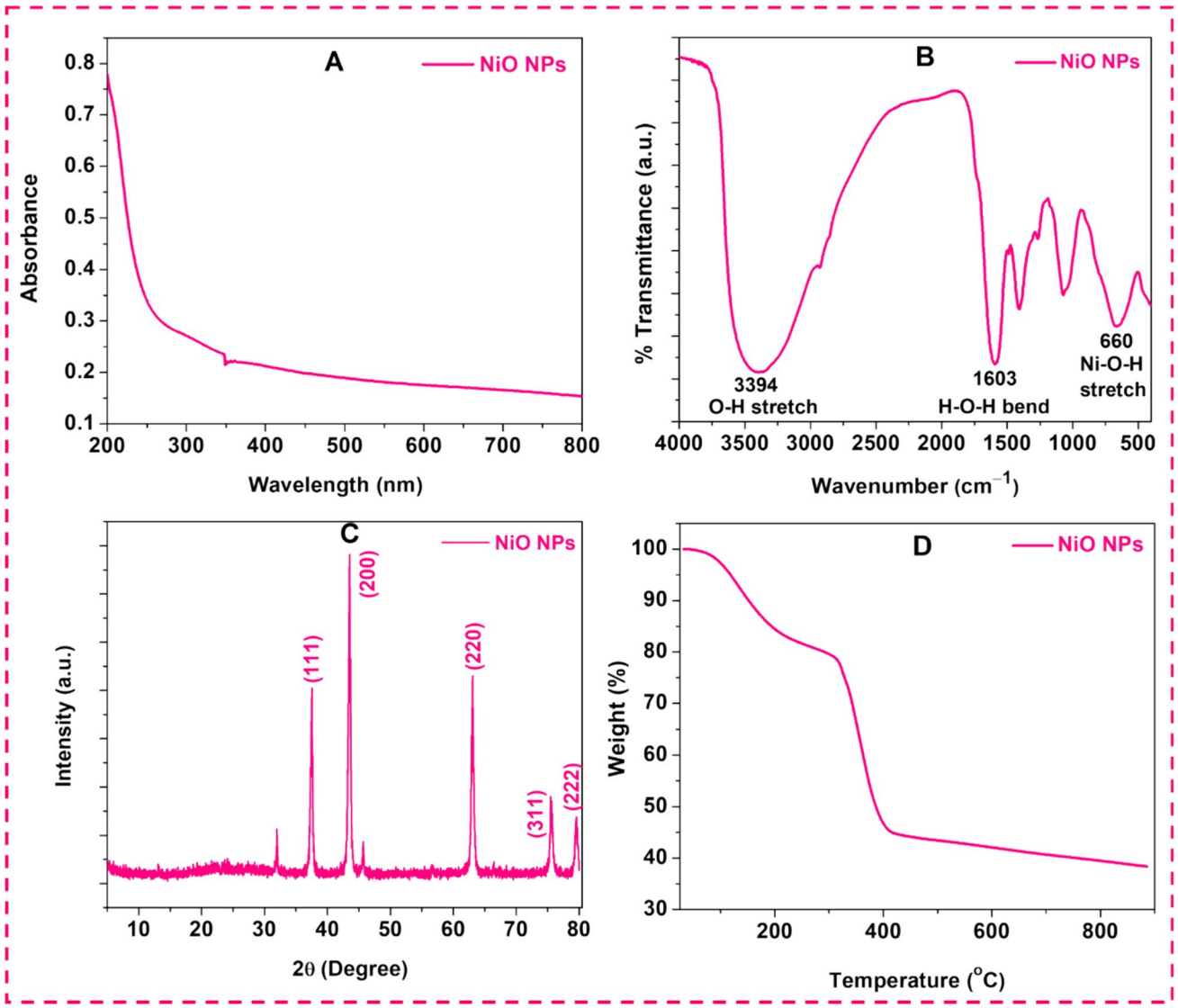

Fig. 1 Green synthesis of NiO NPs from pineapple peel extract. **A** UV–Vis spectrum, **B** FTIR spectrum, **C** XRD profile, and **D** TGA thermogram of synthesized NiO NPs

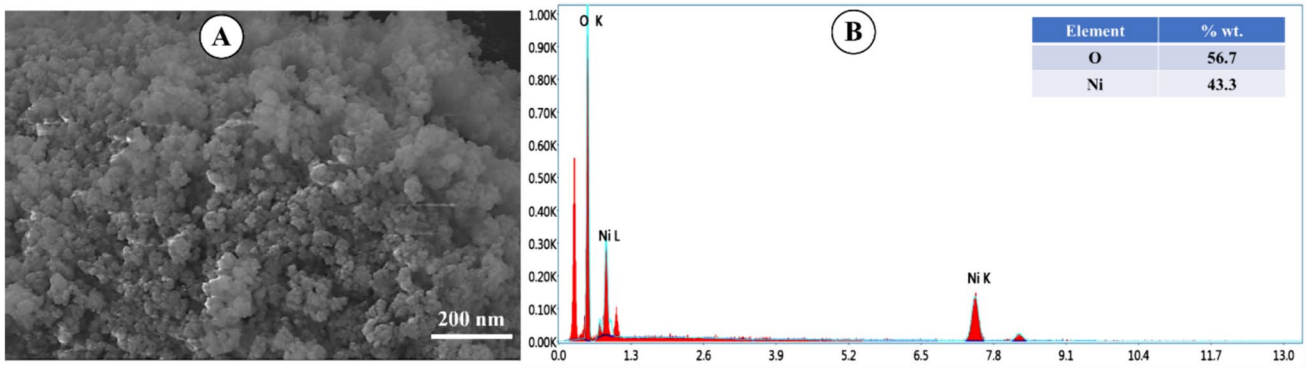

Fig. 2 **A** FESEM image (Scale bar = 200 nm) and **B** EDS of green-synthesized NiO NPs from pineapple peel extract

FTIR analyses of nanocomposite hydrogel

The FTIR spectra of PVA, alginate, PVALg, and PVALg@ NiO have been shown in Fig. 3A. The typical IR absorption bands of PVA were marked at 3400 cm^{-1}, 2930 cm^{-1} and 1720 cm^{-1} corresponded to hydroxyl stretching, C–H stretching from $–CH_2$ groups and the stretching from C = O groups, respectively [37]. The band at 1318 cm^{-1} was ascribed to the hydroxyl bending while those at 922 cm^{-1} and 840 cm^{-1} could be assigned to the CH_2 bending and CH swing [38]. The FTIR spectrum of pristine alginate powder showed key bands at 3440 cm^{-1} and 2920 cm^{-1} attributed to hydroxyl stretching and stretching from $–CH_2$ groups. The symmetric and asymmetric stretching of C–O–C groups were evident at 1615 and 1416 cm^{-1}, respectively. On the other hand, the FTIR spectra of PVALg and PVALg@ NiO hydrogels revealed the presence of the key peaks of both PVA and alginate indicating good interpolymer interaction [37]. Particularly for the nanocomposite hydrogel, the NiO peak at 660 and 620 cm^{-1} was observed and a flattening of the hydroxyl band was witnessed. This could likely be due to the interaction of the O–H groups of the hydrogel with NiO NPs [39]. These spectral data were affirmative of the hydrogel formation and incorporation of nano NiO in the nanocomposite hydrogel.

Thermal analysis of nanocomposite hydrogel

Figure 3B elucidates the TGA plots of PVALg and PVALg@ NiO hydrogels. In the thermogram, PVALg exhibited two steps of weight loss; the first loss around 110 °C is due to the loss of moisture from the hydrogel specimen. The second mass loss occurred around 210–400 °C. This mass loss is associated with the degradation of the polymeric chain. Compared with the PVALg hydrogel, the PVALg@ NiO nanocomposite base hydrogel also exhibited similar type of thermal behavior. In case of PVALg@ NiO hydrogel, the initial mass loss was observed at 110 °C and second mass loss at 430 °C. However, it was observed that the maximum decomposition temperature (T_{max}) was higher for PVALg@ NiO hydrogel in comparison to the pristine PVALg hydrogel. For PVALg hydrogel, the T_{max} revealed around 213 °C, while that for PVALg@ NiO hydrogel was noted at 235 °C. Thus, it could be inferred that the presence of NiO nanostructures has bestowed a slight better thermal stability to the nanocomposite hydrogel in contrast to pristine film [40].

Morphology of hydrogels

The morphology of the hydrogels was visualized through FESEM and the elemental analysis was performed with EDS. The morphology of the PVALg and PVALg@ NiO hydrogels have been displayed in Fig. 4A, A′, respectively. The images indicate the PVALg and PVALg@ NiO hydrogels possessed interconnected porous network structures. The EDS-elemental mapping (Fig. 4B, B′, C, C′) further acknowledged C, O, and Ni in the nanocomposite hydrogel.

Assessment of catalytic activity of PVALg@ NiO hydrogel nanocatalyst

The catalytic performance of the prepared nanocomposite hydrogel PVALg@ NiO was explored by assessing the reduction reactions of 4-NP, $K_3[Fe(CN)_6]$, rhodamine B (RhB), methyl orange (MO), and malachite green (MG) in the presence of a reducing agent, i.e., $NaBH_4$. The following section discusses the reduction reaction for the aforementioned pollutants along with the kinetics in greater details.

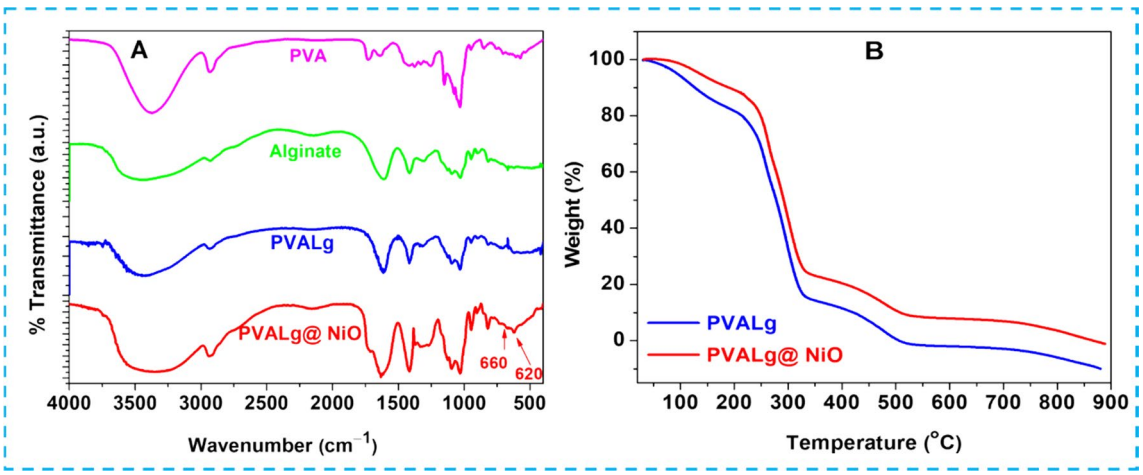

Fig. 3 **A** FTIR spectra of PVA, alginate, PVALg hydrogel and PVALg@ NiO nanocomposite hydrogel. **B** TGA thermograms of PVALg hydrogel and PVALg@ NiO nanocomposite hydrogel

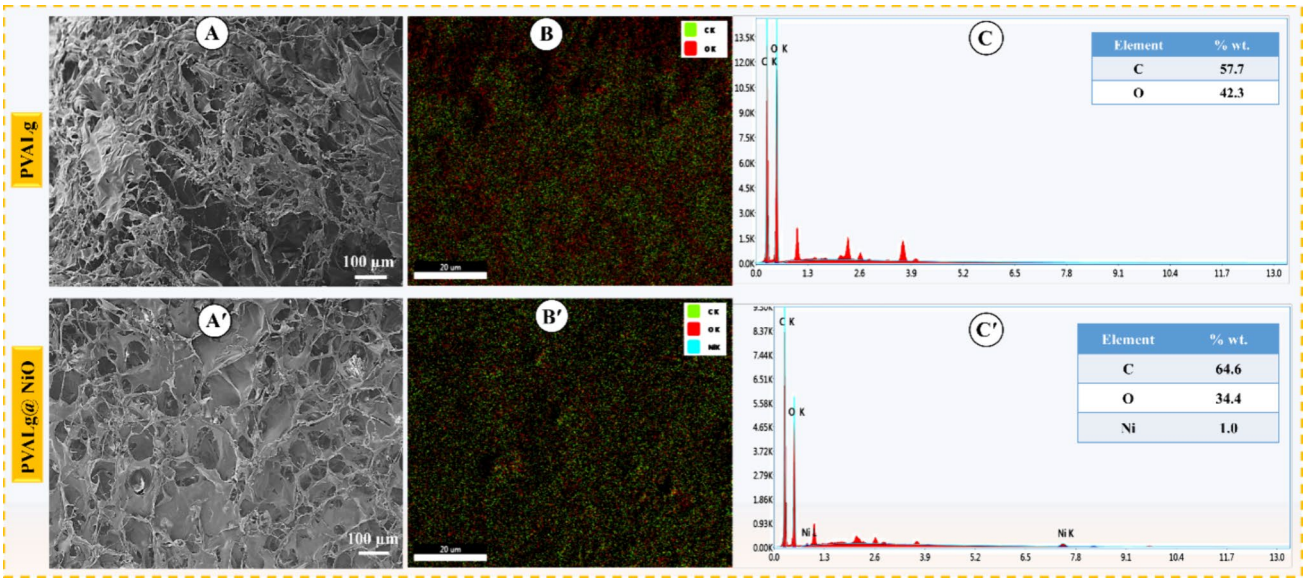

Fig. 4 **A**, **A′** FESEM images (*Scale bar* 100 µm), **B**, **B′** elemental mapping (*Scale bar* 20 µm) and **C**, **C′** EDS of PVALg and PVALg@ NiO nanocomposite hydrogel

The plausible mechanism of reduction has also been presented in the later sections.

Reduction of 4-NP by PVALg@ NiO hydrogel nanocatalyst

The efficacy of the PVALg@ NiO hydrogel nanocatalyst was examined for 4-NP reduction. From Fig. 5A, it was evident that pristine 4-NP displayed an absorption band at 317 nm and visually appeared faint yellowish. After addition of $NaBH_4$ solution, the absorbance shifted to 400 nm and a bright yellow coloration was witnessed. These changes are quite common features in 4-NP reduction owing to the formation of 4-nitrophenolate ions. Herein, the hydride ions of $NaBH_4$ take up the easily available hydrogen from 4-NP and produce hydrogen and 4-nitrophenolate ions. However, further conversion to 4-aminophenol (4-AP) by $NaBH_4$ is an extraordinarily time-consuming process, even though an excess of $NaBH_4$ is utilized. This clearly warrants the employment of both an efficient and sustainable catalyst for the reduction of 4-NP. In this context, green-synthesized metal/metal oxide nanoparticles have been widely recognized for their catalytic potential toward efficient reduction of 4-NP to 4-AP [41]. In our case, the PVALg@ NiO hydrogel served the above purpose. From Fig. 5A, it was seen the absorption peak at 400 nm decreased gradually and almost vanished within a span of 4.0 min after adding the PVALg@ NiO nanocatalyst. This spectral behavior indicated the reduction of 4-NP and that this reaction was completed by 4.0 min.

To optimize the reduction parameters further; the amount of catalyst, 4-NP, $NaBH_4$ were varied. From Fig. 5B–D; the optimized content for 4-NP, catalyst and reducing agent were noted to be 0.5 mM, 30 mg, and 500 mg, respectively, for a reaction period of 4.0 min. The improved catalytic activity of PVALg@ NiO nanocatalyst could likely be accredited to the interactions between hydrogel and NiO NPs. This, in turn, increases the rate of electron transfer and subsequently, facilitates the electron transfer from borohydride to 4-NP through the nanocatalyst. The generally accepted reduction reaction of 4-NP to 4-AP involves the dissolution of $NaBH_4$ followed by ionization in aqueous media to generate BH_4^- ions that react with the composites surface and transfer surface-hydrogen species required for the reduction of 4-NP [42–44]. Overall, the conversion of 4-NP to 4-AP can be summarized in three steps: (i) the adsorption of 4-NP and BH_4^- molecules into the external surface of PVALg@ NiO hydrogel, (ii) transfer of electrons from BH_4^- to 4-NP via the PVALg@ NiO hydrogel, and (iii) the desorption of 4-AP and regeneration of PVALg@ NiO hydrogel. This reduction is a 6-electron transfer process, where the electrons are transferred from BH_4^- to substrate via adsorption onto the catalyst surface. The catalyst aids in the electron relay process, thereby facilitating the reaction between BH_4^- and 4-nitrophenolate anion and subsequently the formation of 4-AP. The mechanism of 4-NP reduction 4-AP by PVALg@ NiO hydrogel nanocatalyst is depicted in Scheme 2.

The recyclability of any catalyst is a crucial feature validating its economic importance. Hence, the recyclability of synthesized PVALg@ NiO hydrogel nanocatalyst was studied. After each batch of 4-NP reduction test, the catalyst was collected, washed thrice with distilled water, dried, and reutilized for the next run. Herein, the recycled hydrogel film

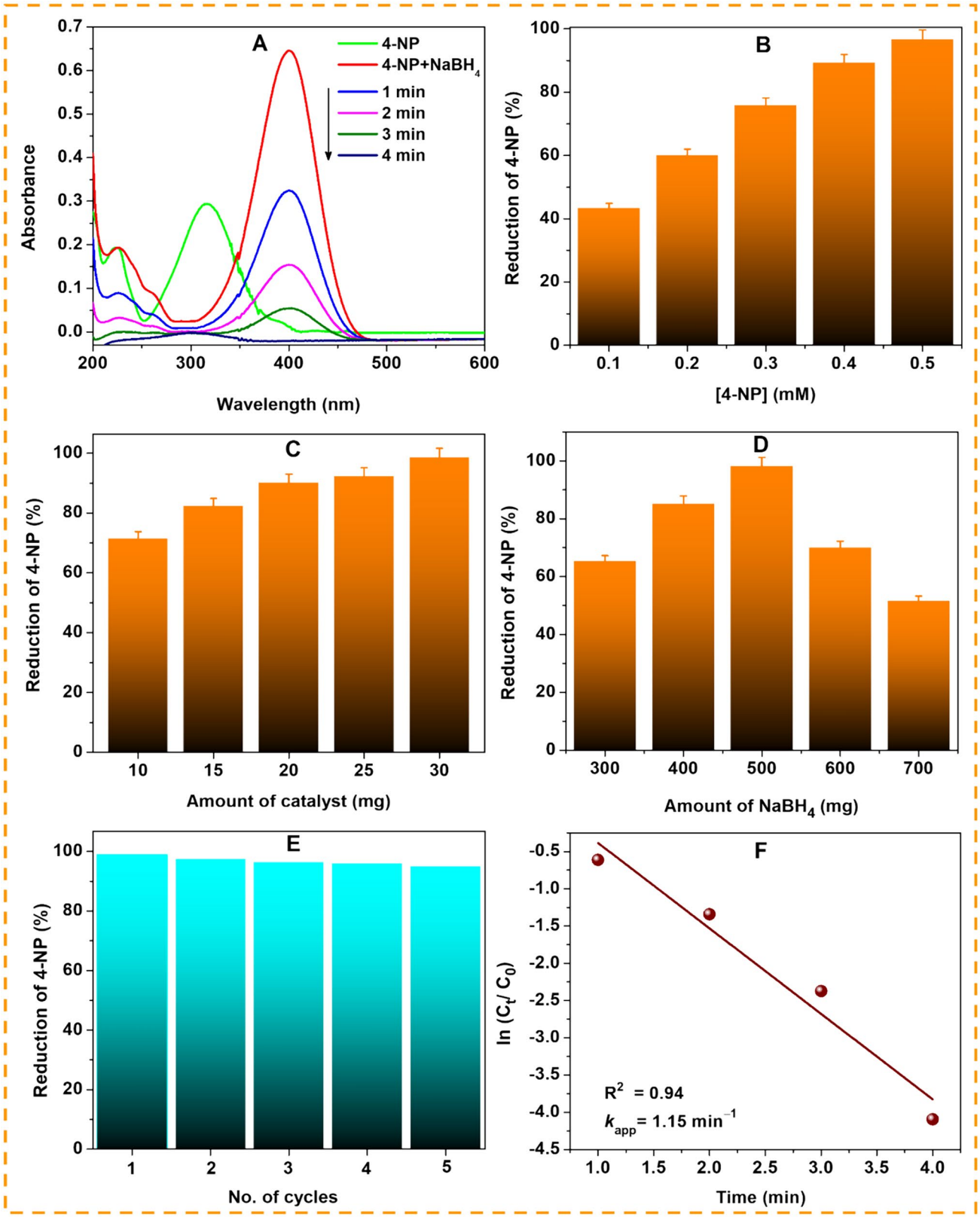

Fig. 5 The catalytic reduction of 4-NP by PVALg@ NiO hydrogel nanocatalyst. **A** UV–Vis spectra of 4-NP with hydrogel as a function of time. Effect of **B** amount of catalyst, **C** amount of $NaBH_4$, **D** concentration of 4-NP and **E** reusability efficacy. **F** Pseudo-first-order kinetic plot for 4-NP reduction by PVALg@ NiO hydrogel nanocatalyst

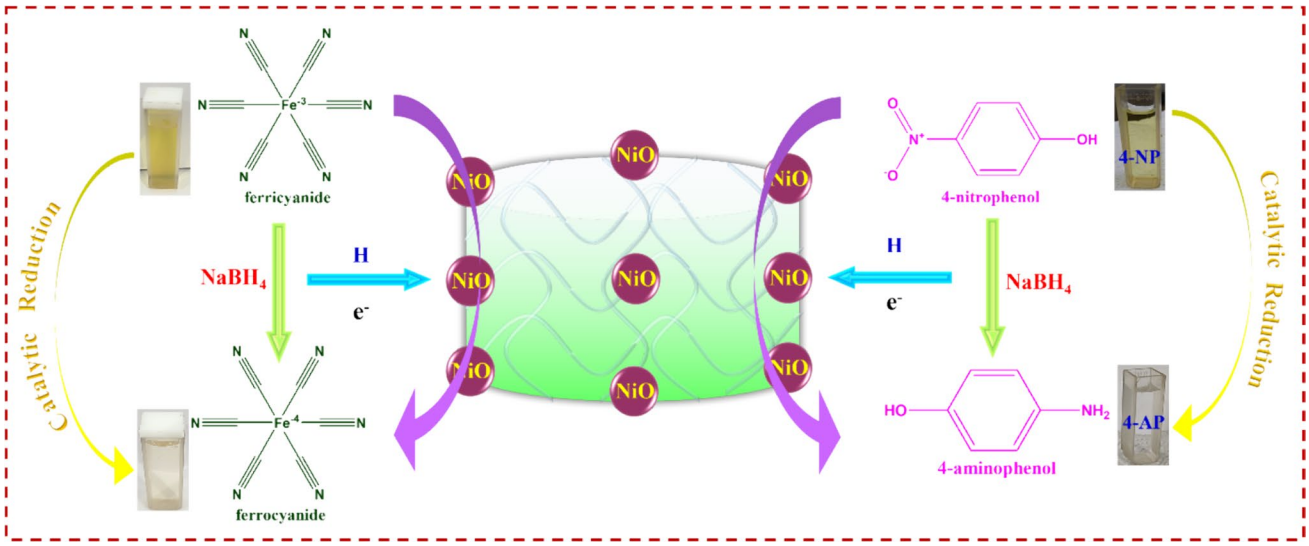

Scheme 2 Schematic and mechanistic illustration of catalytic reduction of 4-NP and potassium hexacyanoferrate (III) by PVALg@ NiO hydrogel nanocatalyst

was re-tested on a new batch of 4-NP and $NaBH_4$. Figure 5E indicates the reduction mettle of 4-NP in each cycle with the same nanocatalyst. The performance of the designed nanocatalyst greatly signified its stability where it remained effectual to almost 95% till the 5th cycle. The results suggest that PVALg@ NiO hydrogel nanocatalyst can be utilized fruitfully for five cycles with any noticeable damage in its catalytic performance.

The pseudo-first-order kinetics was applied for the determination of the rate constant (k_{app}) of reduction of 4-NP by the hydrogel nanocatalyst. The linear relationship of reaction time (t) vs. ln (C_t/C_0) was calculated for 4-NP reduction by PVALg@ NiO hydrogel nanocatalyst and the plots has been presented in Fig. 5F. The rate constant (k_{app}) for catalytic reduction of 4-NP by the hydrogel nanocatalyst was estimated to be 1.15 min^{-1}.

Reduction of $K_3[Fe(CN)_6]$ by PVALg@ NiO hydrogel nanocatalyst

Potassium hexacyanoferrate (III) ($K_3[Fe(CN)_6]$) is a ubiquitous pollutant found in wastewater effluents of gold mining, metal/steel processing and photographic processing applications. It easily finds its way into living organisms including humans via the food chains. Thus, reduction of the Fe(III) to Fe(II) is usually warranted. The efficacy of the PVALg@ NiO hydrogel nanocatalyst was also explored for the reduction of potassium hexacyanoferrate (III) spectrophotometrically by measuring λ_{max} corresponding to 418 nm. After addition of $NaBH_4$ solution, a negligible decrease in absorbance was observed, even after a span of 30 min. This suggested that $NaBH_4$ alone lacks the desired reduction potential for potassium hexacyanoferrate (III). Hence, the reduction was performed using our fabricated hydrogel nanocatalyst PVALg@ NiO. From Fig. 6A, it was seen that the designated peak gradually vanished within a span of 3.0 min with addition of PVALg@ NiO hydrogel nanocatalyst. Furthermore, the original yellow color disappeared after 3.0 min that clearly indicated the formation of $[Fe(CN)_6]^{4-}$. The mechanism of reduction using PVALg@ NiO hydrogel is exhibited in Scheme 2.

We have further optimized the parameters in terms of the content of catalyst, ferricyanide and reducing agent. As noticed from Fig. 6B–D, maximum reduction for 2.0 mM of potassium ferricyanide was noted while using 30 mg catalyst and 500 mg of reducing agent for 3.0 min. The performance of the designed PVALg@ NiO hydrogel nanocatalyst was explored for its recyclability and stability after five individual run cycles. As represented in Fig. 6E, the catalytic reduction of ferricyanide amounted to almost 88% till 5th cycle. The result recommends that PVALg@ NiO hydrogel nanocatalyst can be employed productively for five cycles in the catalytic reduction of potassium hexacyanoferrate (III). The apparent rate constant (k_{app}) for the aforementioned reduction process was estimated from Eq. (1) and found to be 2.15 min^{-1} (Fig. 6F).

A comparative study between the synthesized PVALg@ NiO hydrogel nanocatalyst and other catalysts reported earlier is listed in Table 1. The results clearly demonstrate higher catalytic performance of our designed compared to the reported ones.

Reduction of RhB, MG, and MO by PVALg@ NiO hydrogel nanocatalyst

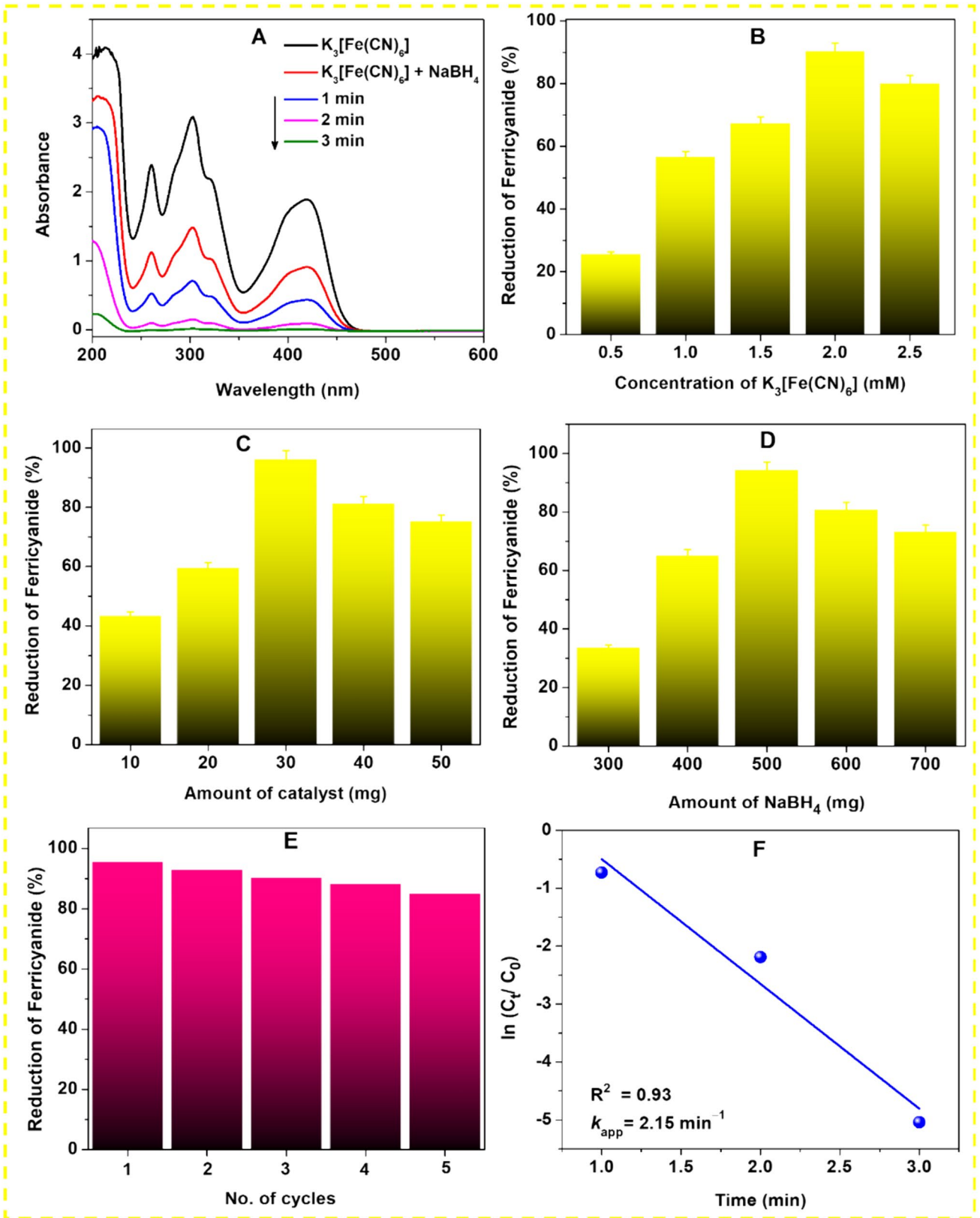

Fig. 6 The catalytic reduction of potassium hexacyanoferrate (III) by PVALg@ NiO hydrogel nanocatalyst. **A** UV–Vis spectra of 4-NP with hydrogel as a function of time. Effect of **B** amount of catalyst, **C** amount of $NaBH_4$, **D** concentration of hexacyanoferrate (III) and **E** reusability efficacy. **F** Pseudo-first-order kinetic plot for potassium hexacyanoferrate (III) reduction by PVALg@ NiO hydrogel nanocatalyst

Table 1 Summary of other catalysts and PVALg@ NiO hydrogel nanocatalyst in reduction of 4-NP and potassium hexacyanoferrate (III)

Pollutant	Catalyst	Catalyst amount	[$NaBH_4$] (M)	Time (min)	References
4-NP (0.13 M)	Alg/CuO–SnO_2	–	0.1	4	[17]
4-NP (0.13 M)	Alg@Cu_2O–Sb_2O_3	10 mg	0.1	3	[45]
4-NP (0.1 mM)	Cu@Alg–FeNi	–	0.01	3	[46]
4-NP (0.13 M)	Cu–Ni sponge	20 mg	0.2	16	[47]
4-NP (10 mM)	Ag@Alg	3 beads	0.05	11	[48]
4-NP (0.5 mM)	PVALg@ NiO	30 mg	0.1	4	This work
$K_3[Fe(CN)_6]$ (2.0 mM)	Alg@Cu_2O–Sb_2O_3	10 mg	0.1	3	[45]
$K_3[Fe(CN)_6]$ (3.0 mM)	Cu NPs–Fe_3O_4–Alg	10 mg	0.25	35 s	[49]
$K_3[Fe(CN)_6]$ (2.0 mM)	Alg@tin oxide–cobalt oxide	10 mg	0.1	5	[50]
$K_3[Fe(CN)_6]$ (2.0 mM)	$SnLa_2O_5$/CMC–Alg	10 mg	0.1	4	[51]
$K_3[Fe(CN)_6]$ (2.0 mM)	PVALg@ NiO	30 mg	0.1	3	This work

Alg alginate, *CMC* carboxymethylcellulose

Catalytic reduction of RhB, MG, and MO in the presence of $NaBH_4$ was also inspected to test the performance of PVALg@ NiO hydrogel nanocatalyst. The reactions progress was monitored spectrophotometrically at definite time span. As witnessed from the UV–Vis spectra in Fig. 7; (A) RhB, (B) MG, and (C) MO exhibited λ_{max} at 550, 615, and 465 nm, respectively. However, after the addition of $NaBH_4$ and catalyst, the total reduction of RhB, MG, and MO was accomplished within 45 s, 45 s, and 90 s, respectively. Figure 7A shows the absorption spectra of the reduction of RhB to leuco-rhodamine B (LRhB) catalyzed by PVALg@ NiO hydrogel nanocatalyst in the presence of $NaBH_4$. From Fig. 7A, the characteristic band of RhB at 550 nm vanished in just 45 s after adding 7.0 mg catalyst, validating its high catalytic activity for RhB (bright pink–red color) transforming to LRhB (colorless). Figure 7B illustrates the serial absorption spectra of the reduction of MG with 5.0 mg of PVALg@ NiO hydrogel nanocatalyst. From Fig. 7B, it was clearly evident that the key peak of MG at 615 nm dropped to zero within 45 s of reaction time to complete the transformation of MG to leuco-malachite green (LMG). The formation of LMG (colorless) within 45 s of reaction time recommend the greater catalytic potency of PVALg@ NiO hydrogel nanocatalyst. For the reduction reactions of RhB and MG, the aforesaid dyes act as electrophile with respect to the PVALg@ NiO hydrogel nanocatalyst, while the BH_4^- serves as the electron donor (nucleophile). Thus, the nucleophilic borohydride can offer its electrons to the catalyst whence the electrophilic dyes can receive these electrons from the catalyst. In other words, PVALg@ NiO hydrogel nanocatalyst behaves as an electron relay for RhB and MG reduction in $NaBH_4$ solution [52, 53]. Figure 7C displays the UV–Vis absorption spectra of the reduction of MO catalyzed by 7.0 mg PVALg@ NiO hydrogel nanocatalyst in the presence of $NaBH_4$. From the spectra, the key band of MO at 465 nm disappeared in 90 s after adding a 7.0 mg catalyst, confirming its catalytic activity for MO (bright orange color) to forming degraded products (colorless). These results reveal that the azo group in MO get reduced in the presence of BH_4^- and nanocatalyst. Both the MO and borohydride adsorb on the surface of hydrogel nanocatalyst which facilitates the electron transfer from BH_4^- to MO; thereby aiding in the reduction of azo bonds (–N=N–) to (–N–N–) bonds, and finally the forming the colorless degraded products [17, 50]. The optimized catalyst loading on the reduction times of the aforesaid dyes have been projected in Table 2. The plausible scheme of reduction of RhB, MG and MO dyes by the PVALg@ NiO hydrogel nanocatalyst has been projected in Scheme 3. The pseudo-first order kinetics was applied for the determination of k_{app}. Figure 7D shows plots of ln (C_t/C_0) as a function of reaction time for the reduction of dyes by PVALg@ NiO hydrogel nanocatalyst. The k_{app} values found to be 0.17 s^{-1}, 0.17 s^{-1} and 0.05 s^{-1} for RhB, MG, and MO reduction reactions respectively.

Table 3 presents a comparison between the synthesized PVALg@ NiO nanocatalyst with other reported catalysts for reduction of RhB, MG, and MO dyes.

Catalyst recyclability

The reusability of PVALg@ NiO hydrogel nanocatalyst was investigated toward the reduction of RhB. As depicted in Fig. 8A, the catalyst performance notably signified the stability and recyclability of the PVALg@ NiO hydrogel nanocatalyst till 4th run. It was further realized that the performance decreased gradually with the increased number of runs. This might be attributed to the diminution in the activity sites of the catalyst [60, 61]. Furthermore, the structure of the recycled catalyst was investigated by XRD. Figure 8B depicts the XRD patterns of PVALg@ NiO before and after four experimental runs. No noticeable change in intensity

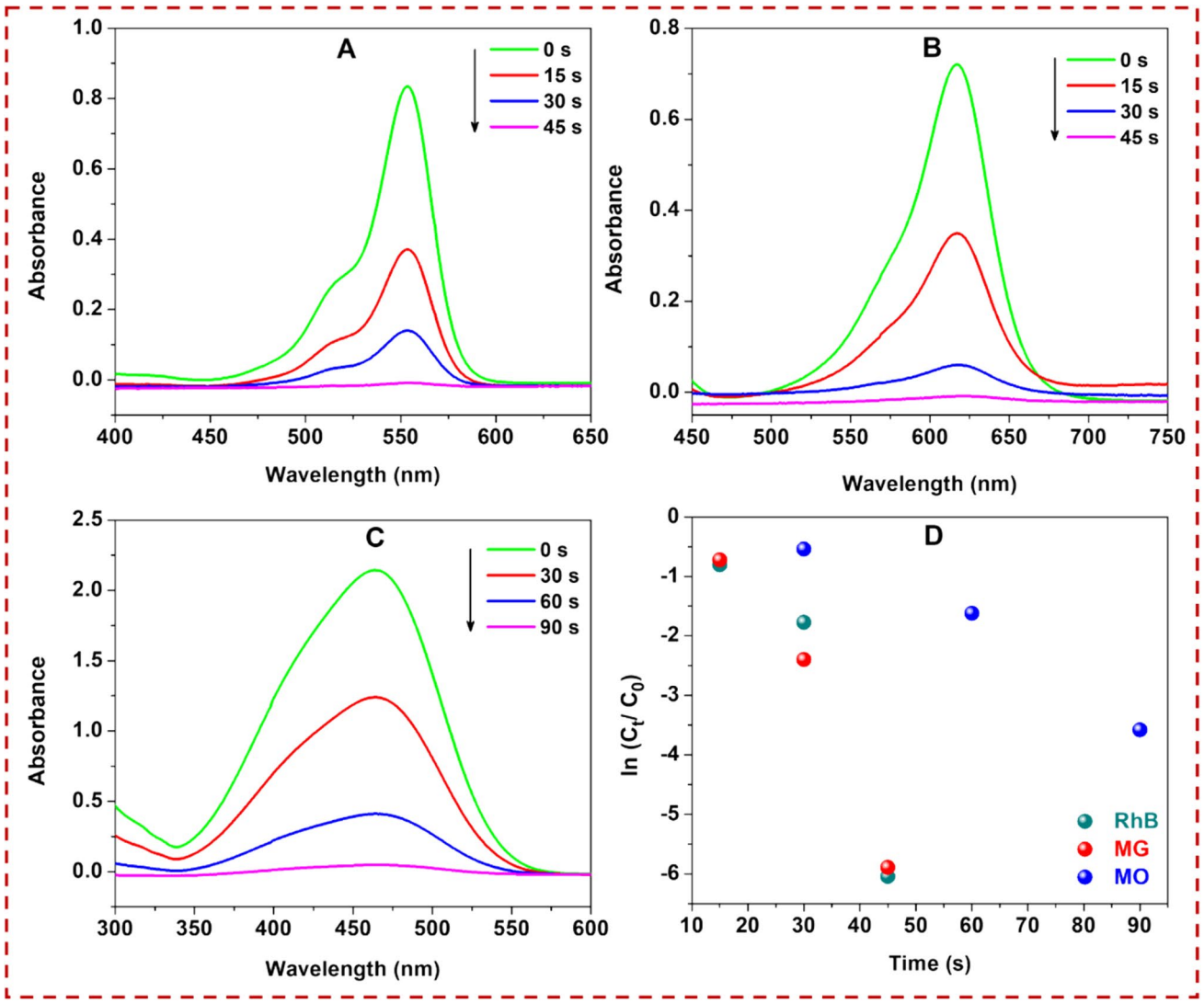

Fig. 7 UV–Vis spectra for reduction of **A** RhB, **B** MG, and **C** MO with PVALg@ NiO hydrogel nanocatalyst. **D** Pseudo-first-order kinetic plots for dyes reduction by PVALg@ NiO hydrogel nanocatalyst

Table 2 Optimized parameters of PVALg@ NiO hydrogel nanocatalyst loading on the reduction of RhB, MG, and MO

Sl. No	Dye	Catalyst (mg)	Time (s)
1	RhB (2.0×10^{-5} M)	3.0	150
		5.0	90
		7.0	45
2	MG (2.0×10^{-5} M)	3.0	90
		5.0	45
		7.0	Immediately
3	MO (2.5×10^{-5} M)	3.0	120
		5.0	90
		7.0	Immediately

Reaction conditions: dyes (25 mL), $NaBH_4$ (0.1 M), room temperature

was marked from the XRD data. The structure and crystalline phase also remained intact after the catalytic reduction. Furthermore, the FTIR spectra presented in Fig. 8C suggested that no major changes were incurred by the hydrogel catalyst after the experiments. No new peaks could be noted rather a broadening of the hydroxyl stretching around 3500 cm^{-1} was evident. This could be rationalized by considering the four runs of the hydrogel for RhB reduction in aqueous medium. Additionally, the morphology of the catalyst was further visualized after the catalytic four runs and the images are shown in Fig. 8D. A slight reduction in porosity of the PVALg@ NiO was evidenced post-catalysis four runs. This could be attributed to the diminution in the activity sites of the catalyst which decreased gradually with each run. Nonetheless, the aforesaid results suggested that the PVALg@ NiO catalyst is stable during reduction

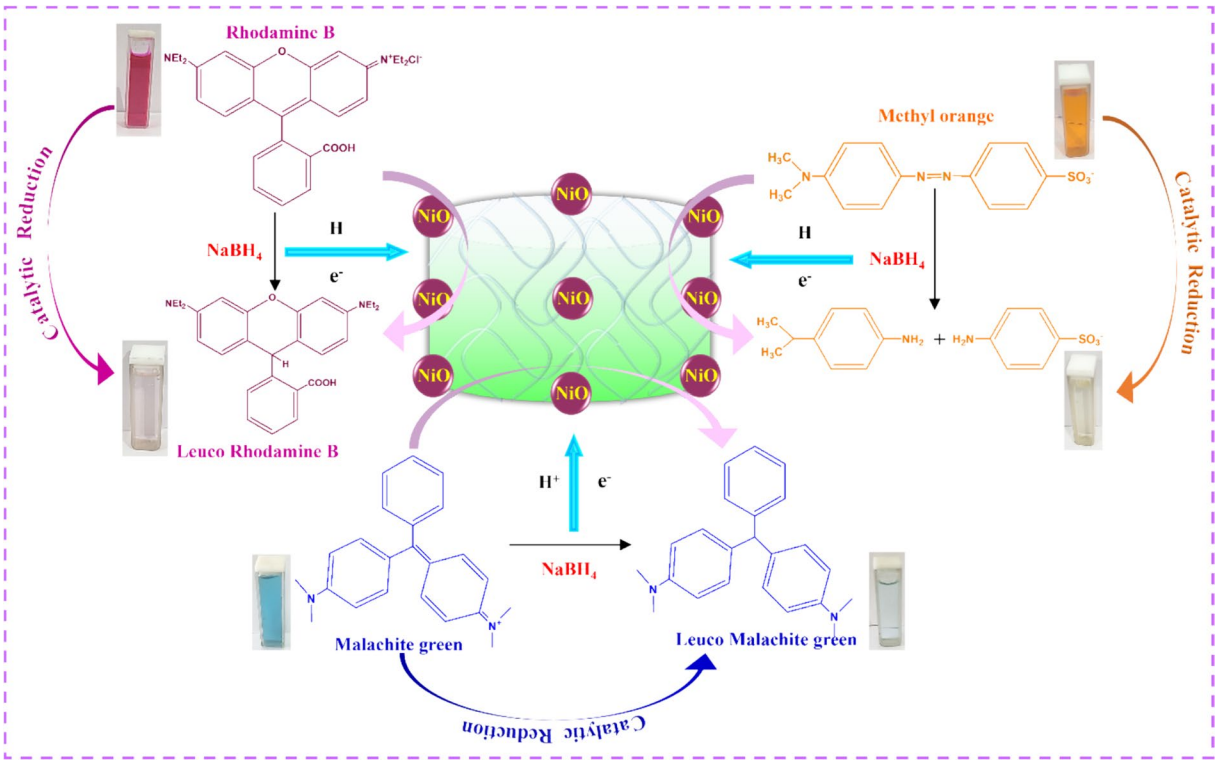

Scheme 3 Schematic and mechanistic illustration of catalytic reduction of dyes by PVALg@ NiO hydrogel nanocatalyst

Table 3 Summary of other catalysts and PVALg@ NiO hydrogel nanocatalyst in reduction in reduction of RhB, MG, and MO dyes

Dye	Catalyst	Catalyst amount	$NaBH_4$	Time	References
RhB (2.09×10^{-5} M)	Pd NPs/Fe_3O_4@nanocellulose	10 mg	5.3 mM	110 s	[54]
RhB (1.75×10^{-5} M)	CuNiOS-0.6	–	0.1 M	60 s	[52]
RhB (2.0×10^{-5} M)	PVALg@ NiO	7.0 mg	0.1 M	45 s	This work
MG (5.0×10^{-3} M)	Ag NPs	0.01 M	0.5 M	30 min	[55]
MG (3.0×10^{-3} M)	Ag–P(NAA)	0.02 mL	1.5 mM	6 min	[56]
MG	rGO-PANI/Pd-Au	–	–	30 min	[57]
MG (2.0×10^{-5} M)	PVALg@ NiO	7.0 mg	0.1 M	Immediate	This work
MO (5.0×10^{-3} M)	Au NPs	0.01%	0.5 M	40 min	[58]
MO (20.1 mg/L)	Co Nanocomposite	1 mg/mL	4 mg	7 min	[59]
MO (2.5×10^{-5} M)	PVALg@ NiO	7.0 mg	0.1 M	Immediate	This work

process and is economically viable for large-scale industrial applications.

Efficacy of PVALg@ NiO hydrogel nanocatalyst *in real* samples

To further explore the efficacy of our synthesized PVALg@ NiO hydrogel nanocatalyst toward dye reduction in real specimen, we have prepared the stock solutions of RhB, MG, and MO from waters of our university, student hostel, and a nearby local pond. The optimized concentrations of the respective dyes, reducing agent, and the catalyst were maintained as mentioned in Table 2. The times of reduction of the dyes with the water samples were recorded and are listed in Table 4. The reduction of RhB was accomplished in 2.0 min for water samples collected from university and local pond while the time span was 3.0 min upon treatment with hostel water. For MG; reduction could be achieved at 3.0 min for water samples from university and hostel; yet, the process sped up on using water from pond. The reduction of MO in university water,

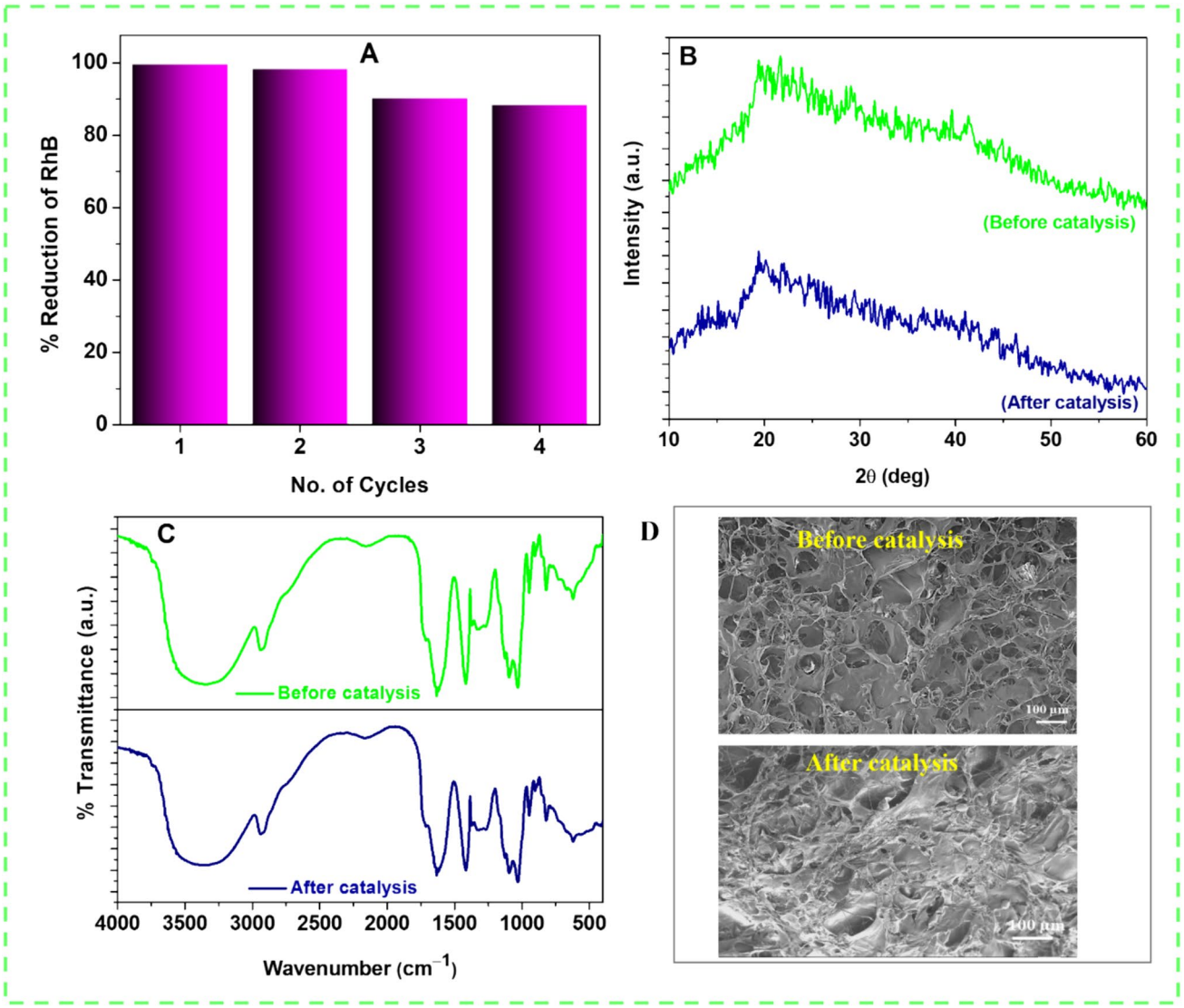

Fig. 8 **A** Recyclability of PVALg@ NiO hydrogel nanocatalyst for RhB reduction. **B** XRD profile, **C** FTIR spectra and **D** FESEM images of recycled PVALg@ NiO hydrogel nanocatalyst

Table 4 The catalytic reduction potential of PVALg@ NiO hydrogel nanocatalyst on different dyes in real water samples

Samples→ Dyes↓	University water		Hostel water		Local pond water	
	Reduction (%)	Time (min)	Reduction (%)	Time (min)	Reduction (%)	Time (min)
RhB	98.5	2.0	96.5	3.0	98.0	2.0
MG	91.3	3.0	95.6	3.0	96.4	1.5
MO	93.2	4.0	92.5	3.0	92.3	3.0

hostel water, and pond water were obtained at 4.0, 3.0, and 3.0 min, respectively. Altogether, Table 4 reflects the high reduction potency of our prepared PVALg@ NiO hydrogel nanocatalyst on RhB, MO, and MG dyes in real water samples.

Conclusion

This study puts forth the efficacy of green-synthesized NiO NPs-integrated PVA–alginate nanocomposite hydrogels as potent catalyst for reduction of hazardous anthropogenic water pollutants. The biogenic synthesis of the NPs was

accomplished from waste pineapple peel extract. The extraction was accomplished via the microwave-assisted method which is environmentally benign. The formation of NiO nanostructures was ascertained from different analytical techniques such as UV–Vis, FTIR, XRD, TGA, FESEM, and EDS. Spherical NiO NPs were visualized having an average particle size of 11.5 nm (from Scherrer formula). Hydrogels composed of PVA, alginate and NiO nanoparticles were synthesized via the simple facile strategy of solvent casting. The thermal analyses of the hydrogel indicated that NiO NPs have rendered an enhanced stability to the PVALg@ NiO hydrogel. The synthesized PVALg@ NiO hydrogel was utilized as a catalyst in the reduction of common hazardous water pollutants namely 4-nitrophenol, potassium hexacyanoferrate (III), and organic dyes rhodamine B, malachite green, methyl orange in the presence of a reducing agent, i.e., $NaBH_4$. The influence of different parameters on the catalytic activity and the kinetics were assessed in greater details. Under optimized conditions, the rate constant for 4-NP and potassium hexacyanoferrate (III) reduction was estimated to be 1.15 min^{-1} and 2.15 min^{-1} for 30 mg of catalyst. The rate of reduction was found to be faster for the dyes employed and the respective rate constants were be 0.17 s^{-1} for RhB, MG and 0.05 s^{-1} for MO, respectively. The efficacy of the PVALg@ NiO hydrogel nanocatalyst was further examined for the reduction of dyes in real water samples collected from three different sources. The reduction reactions of RhB and MG was accomplished by 3.0 min while that for MO was noted to be 4.0 min. The recyclability and stability studies validate the efficacy of the PVALg@ NiO hydrogel nanocatalyst till the 4th run with no perceptible diminution in its catalytic activity.

In summary, this study validates two meritorious prospects: (i) valorization of waste pineapple peel toward the green synthesis of nanoparticles and (ii) a sustainable hydrogel nanocatalyst for efficient reduction of hazardous anthropogenic water pollutants including organic dyes.

Acknowledgements The authors acknowledge Department of Chemistry, Odisha University of Technology and Research, Bhubaneswar and Department of Chemistry, Ravenshaw University, Cuttack for providing the necessary facilities required for the study.

Author contributions GD: Conceptualization, investigation, writing original draft. MJ, DJ, NK, MSSP, AS: Investigation, formal analysis. BRD: Conceptualization, investigation, formal analysis, supervision. SD: Conceptualization, supervision, writing—review and editing.

Funding No funding was received for conducting this study.

Data availability The authors declare that the data supporting the findings in this study are presented within the paper. The data are also available from the corresponding author upon request.

Declarations

Conflict of interest The authors have no competing interests to declare that are relevant to the content of this article.

Consent for publication All the authors gave their consent to publish this work.

References

1. Dadashi J, Ghasemzadeh MA, Salavati-Niasari M (2022) Recent developments in hydrogels containing copper and palladium for the catalytic reduction/degradation of organic pollutants. RSC Adv 12:23481–23502
2. Alwan SH, Alshamsi HA (2022) In situ synthesis NiO/F-MWCNTs nanocomposite for adsorption of malachite green dye from polluted water. Carbon Lett 32:1073–1084
3. Allah MAAH, Alshamsi HA (2023) Green synthesis of AC/ZnO nanocomposites for adsorptive removal of organic dyes from aqueous solution. Inorg Chem Commun 157:111415
4. Khoo YS et al (2022) Removal of emerging organic micropollutants via modified-reverse osmosis/nanofiltration membranes: a review. Chemosphere 305:135151
5. Tang X et al (2016) Chemical coagulation process for the removal of heavy metals from water: a review. Desalin Water Treat 57:1733–1748
6. Al-nayili A, Muhammad AJ (2023) Perovskite's $LaNiMnO_6$/montmorillonite K10 nanocomposites: synthesis and enhanced photocatalytic activity. Mater Sci Semicond Process 155:107254
7. Ahmed A, Alabada R, Usman M, Alothman AA, Tufail MK, Mohammad S, Ahmad Z (2024) Synthesis of visible-light-responsive lanthanum-doped copper ferrite/graphitic carbon nitride composites for the photocatalytic degradation of toxic organic pollutants. Diam Rel Mater 141:110630
8. Bibi F et al (2024) Fabrication of Ni and Mn co-doped $ZnFe_2O_4$ spinel ferrites and their nanocomposites with rGO as an efficient photocatalyst for the remediation of organic dyes. Polyhedron 250:116826
9. Ahmed D et al (2023) Efficient degradation of atrazine from synthetic water through photocatalytic activity supported by titanium dioxide nanoparticles. Z Phys Chem 237:395–412
10. Usman M, Ahmed A, Hu Z-F, Shen Y-Q, Yu B, Cong H-L (2019) Synthesis, characterization and photocatalytic activity of iron nanoparticles from *Ficus carica* peels via biological method. Ferroelectrics 548:89–96
11. Rasalingam S, Peng R, Koodali RT (2014) Removal of hazardous pollutants from wastewaters: applications of TiO_2-SiO_2 mixed oxide materials. J Nanomater 617405:2014
12. Din MI, Khalid R, Hussain T, Mujahid A, Najeeb J, Izhar F (2020) Nanocatalytic assemblies for catalytic reduction of nitrophenols: a critical review. Crit Rev Anal Chem 50:322–338
13. Ndolomingo MJ, Bingwa N, Meijboom R (2020) Review of supported metal nanoparticles: synthesis methodologies, advantages and application as catalysts. J Mater Sci 55:6195–6241
14. Bashir MS et al (2022) Metallic nanoparticles for catalytic reduction of toxic hexavalent chromium from aqueous medium: a state-of-the-art review. Sci Total Environ 829:154475
15. Naseem K, Farooqi ZH, Begum R, Irfan A (2018) Removal of Congo red dye from aqueous medium by its catalytic reduction using sodium borohydride in the presence of various inorganic nano-catalysts: a review. J Clean Prod 187:296–307
16. Lou Y-Y, Fontmorin J-M, Amrane A, Fourcade F, Geneste F (2021) Metallic nanoparticles for electrocatalytic reduction of

halogenated organic compounds: a review. Electrochim Acta 377:138039
17. Khan SB, Akhtar K, Bakhsh EM, Kamal T, Asiri AM (2022) Alginate biopolymer as a reactor container for copper oxide-tin oxide: efficient nanocatalyst for reduction of different pollutants. Chemosphere 291:132811
18. Lee KY, Mooney DJ (2012) Alginate: properties and biomedical applications. Prog Polym Sci 37:106–126
19. Thakur S, Sharma B, Verma A, Chaudhury J, Tamulevicius S, Thakur VK (2018) Recent progress in sodium alginate based sustainable hydrogels for environmental applications. J Clean Prod 198:143–159
20. Funami T, Fang Y, Noda S, Ishihara S, Nakamura M, Draget K et al (2009) Rheological properties of sodium alginate in an aqueous system during gelation in relation to supermolecular structures and Ca2+ binding. Food Hydrocoll 23:1746–1755
21. Martínez-Gómez F, Guerrero J, Matsuhiro B, Pavez J (2017) In vitro release of metformin hydrochloride from sodium alginate/polyvinyl alcohol hydrogels. Carbohydr Polym 155:182–191
22. Kumar A, Han SS (2017) PVA-based hydrogels for tissue engineering: a review. Int J Polym Mater Polym Biomater 66:159–182
23. Mok CF, Ching YC, Muhamad F et al (2020) Adsorption of dyes using poly(vinyl alcohol) (PVA) and PVA-based polymer composite adsorbents: a review. J Polym Environ 28:775–793
24. Golafshan N, Rezahasani R, Esfahani MT, Kharaziha M, Khorasani SN (2017) Nanohybrid hydrogels of laponite: PVA-Alginate as a potential wound healing material. Carbohydr Polym 176:392–401
25. Yu F et al (2018) Evaluation of a polyvinyl alcohol-alginate based hydrogel for precise 3D bioprinting. J Biomed Mater Res Part A 106:2944–2954
26. Rezagholizade-shirvan A, Najafi MF, Behmadi H, Masrournia M (2022) Preparation of nano-composites based on curcumin/chitosan-PVA-alginate to improve stability, antioxidant, antibacterial and anticancer activity of curcumin. Inorg Chem Commun 145:110022
27. Zhang M-K, Zhang X-H, Han G-Z (2021) Magnetic alginate/PVA hydrogel microspheres with selective adsorption performance for aromatic compounds. Sep Purif Technol 278:119547
28. Yi X, Sun F, Han Z, Han F, He J, Ou M, Gu J, Xu X (2018) Graphene oxide encapsulated polyvinyl alcohol/sodium alginate hydrogel microspheres for Cu (II) and U (VI) removal. Ecotoxicol Environ Saf 158:309–318
29. Karpagavinayagam P, Prasanna AEP, Vedhi C (2022) Eco-friendly synthesis of nickel oxide nanoparticles using *Avicennia Marina* leaf extract: morphological characterization and electrochemical application. Mater Today Proceed 48:136–142
30. Ahmad W, Bhatt SC, Verma M, Kumar V, Kim H (2022) A review on current trends in the green synthesis of nickel oxide nanoparticles, characterizations, and their applications. Environ Nanotechnol Monit Manag 18:100674
31. Jana S, Mondal G, Mitra BC, Bera P, Chakraborty B, Mondal A, Ghosh A (2017) Facile synthesis of nickel oxide thin films from PVP encapsulated nickel sulfide thin films: an efficient material for electrochemical sensing of glucose, hydrogen peroxide and photodegradation of dye. New J Chem 41:14985–14994
32. Xing W, Li L, Yan ZF, Lu GQ (2005) Synthesis and characterization of mesoporous nickel oxide and its application to electrochemical capacitor. Acta Chim Sin 63:1775
33. Kanthimathi M, Dhathathreyan A, Nair BV (2004) Nanosized nickel oxide using bovine serum albumin as template. Mater Lett 58:2914–2917
34. M-ElNagy KN, E-Al M (2013) Nickel oxide nanoparticles: synthesis and spectral studies of interactions with glucose. Mater Sci Semicond Process 16:1747–1752
35. Yung T-Y, Huang L-Y, Chan T-Y, Wang K-S, Liu T-Y, Chen P-T, Chao C-Y, Liu L-K (2014) Synthesis and characterizations of Ni-NiO nanoparticles on PDDA-modified graphene for the oxygen reduction reaction. Nanoscale Res Lett 9:444
36. Sabouri Z, Rangrazi A, Amiri MS et al (2021) Green synthesis of nickel oxide nanoparticles using *Salvia hispanica* L. (chia) seeds extract and studies of their photocatalytic activity and cytotoxicity effects. Bioprocess Biosyst Eng 44:2407–2415
37. Dalei G, Swain S, Das S, Das SP (2020) Controlled release of 5-fluorouracil from alginate hydrogels by cold HMDSO-plasma surface engineering. ChemSelect 5:2168–2178
38. Wang T et al (2020) Polyvinyl alcohol/sodium alginate hydrogels incorporated with silver nanoclusters via green tea extract for antibacterial applications. Des Monomer Polym 23:118–133
39. Khalil A, Ali N, Asiri AM et al (2021) Synthesis and catalytic evaluation of silver@nickel oxide and alginate biopolymer nanocomposite hydrogel beads. Cellulose 28:11299–11313
40. Kamal T, Asiri AM, Ali N (2021) Catalytic reduction of 4-nitrophenol and ethylene blue pollutants in water by copper and nickel nanoparticles decorated polymer sponges. Spectrochim Acta Part A Mol Biomol Spectrosc 261:120019
41. Mejia YR, Bogireddy NKR (2022) Reduction of 4-nitrophenol using green-fabricated metal nanoparticles. RSC Adv 12:18661–18675
42. Priyadarshini SS, Sethi S, Rout S et al (2023) Green synthesis of microalgal biomass-silver nanoparticle composite showing antimicrobial activity and heterogenous catalysis of nitrophenol reduction. Biomass Convers Biorefinery 13:7783–7795
43. Narayanan RK, Devaki SJ (2015) Brawny silver-hydrogel based nanocatalyst for reduction of nitrophenols: studies on kinetics and mechanism. Ind Eng Chem Res 54:1197–1203
44. Ajmal M, Aftab F, Bibi I et al (2019) Facile synthesis of porous anionic hydrogel embedded with nickel nanoparticles and evaluation of its catalytic performance for the rapid reduction of 4-nitrophenol. J Porous Mater 26:281–290
45. Khan SB et al (2022) Copper oxide-antimony oxide entrapped alginate hydrogel as efficient catalyst for selective reduction of 2-nitrophenol. Polymers 14:458
46. Al-Ghamdi YO (2023) Alginate biopolymer FeNi nanocomposite blend stabilizes cu nanoparticles template for hydrogenation of nitrophenol and dyes discoloration. J Polym Environ 31:1812–1827
47. Kamal T, Asiri AM, AM, Ali N, (2021) Catalytic reduction of 4-nitrophenol and methylene blue pollutants in water by copper and nickel nanoparticles decorated polymer sponges. Spectrochim Acta Part A Mol Biomol Spectrosc 261:120019
48. Ai L, Jiang J (2013) Catalytic reduction of 4-nitrophenol by silver nanoparticles stabilized on environmentally benign macroscopic biopolymer hydrogel. Biores Technol 132:374–377
49. Kalantari E, Lucia L, Lavoine N (2022) Green synthesis, characterization, and catalytic application of a supported and magnetically isolable copper-iron oxide-sodium alginate. Green Syn Catal 3:179–184
50. Bakhsh EM, Akhtar K, Fagieh TM, Khan SB, Asiri AM (2021) Development of alginate@tin oxide cobalt oxide nanocomposite-based catalyst for the treatment of wastewater. Int J Biol Macromol 187:386–398
51. Akhtar K, Bakhsh EM, Khan SB, Khan M, Asiri AM (2023) $SnLa_2O_5$ wrapped carboxymethyl cellulose mixed calcium alginate nanocomposite beads for efficient reduction of pollutants. Int J Biol Macromol 233:123564
52. Abay AK, Chen X, D. Kuo D-H, (2017) Highly efficient noble metal free copper nickel oxysulfide nanoparticles for catalytic reduction of 4-nitrophenol, methyl blue, and rhodamine-B organic pollutants. New J Chem 241:5628–5638

53. Ganapuram RB, Alle M, Dadigala R, Dasari A, Maragoni V, Guttena V (2015) Catalytic reduction of methylene blue and Congo red dyes using green synthesized gold nanoparticles capped by *Salmalia malabarica* gum. Int Nano Lett 5:215–222
54. Kalantari E, Khalilzadeh MA, Zareyee D (2021) Effective reduction of Cr(VI) and organic dyes using Pd NPs/Fe_3O_4@nanocellulose as a recoverable catalyst in aqueous media. J Inorg Organomet Polym Mater 31:319–330
55. Matheswari PP, Jeyamalar JI, Asha RN (2019) Green synthesis, characterization and catalytic degradation studies of metal nanoparticles against malachite green. Pharm Innov J 8:968–974
56. Farooqi ZH et al (2022) Catalytic degradation of malachite green using a crosslinked colloidal polymeric system loaded with silver nanoparticles. Int J Environ Anal Chem 102:4104–4120
57. Sivaranjan K, Padmaraj O, Santhanalakshmi J et al (2020) Effect of hybrid mono/bimetallic nanocomposites for an enhancement of catalytic and antimicrobial activities. Sci Rep 10:2586
58. Gupta N, Singh HP, Sharma RK (2011) Metal nanoparticles with high catalytic activity in degradation of methyl orange: an electron relay effect. J Mol Catal A Chem 335:248–252
59. Buhkamsin HA, Hammud HH, Awada C, Prakasam T (2024) Catalytic reductive degradation of 4-nitrophenol and methyl orange by novel cobalt oxide nanocomposites. Catalysts 14:89
60. Che W, Ni Y, Zhang Y, Ma Y (2015) Morphology-controllable synthesis of CuO nanostructures and their catalytic activity for the reduction of 4-nitrophenol. J Phys Chem Solid 77:1–7
61. Huang C, Ye W, Liu Q, Qiu X (2014) Dispersed Cu_2O octahedrons on H-BN nanosheets for p-nitrophenol reduction. ACS Appl Mater Interfaces 6:14469–14476

Authors and Affiliations

Ganeswar Dalei[1] · Monalisa Jena[1] · Debasis Jena[2] · Navneel Kaur[1] · M. Swadhin Shakti Prasad[1] · Ayushman Sahu[1] · Bijnyan Ranjan Das[1] · Subhraseema Das[1,2]

✉ Subhraseema Das
subhraseema@ravenshawuniversity.ac.in;
subhraseema@gmail.com

[1] Department of Chemistry, Odisha University of Technology and Research, Bhubaneswar, Odisha 751029, India

[2] Department of Chemistry, Ravenshaw University, Cuttack, Odisha 753003, India